CHEMISTRY OF MATERIALS

Article

pubs.acs.org/cm

Theoretical Limiting Potentials in Mg/O_2 Batteries

Jeffrey G. Smith,[†] Junichi Naruse,[§] Hidehiko Hiramatsu,[∥] and Donald J. Siegel*[,†,‡,⊥,#]

[†]Mechanical Engineering Department, [‡]Materials Science & Engineering, and [⊥]Michigan Energy Institute, University of Michigan, Ann Arbor, Michigan 48109, United States

[§]North America Research & Development, DENSO International America, Inc., 24777 Denso Drive, Southfield, Michigan 48086, United States

[∥]Research Laboratories, DENSO CORPORATION, 500-1, Minamiyama, Komenoki-cho, Nisshin 470-0111, Japan

[#]Department of Energy Conversion and Storage, Technical University of Denmark, Fysikvej, Building 309, 2800 Kgs Lyngby, Denmark

ABSTRACT: A rechargeable battery based on a multivalent Mg/O_2 couple is an attractive chemistry due to its high theoretical energy density and potential for low cost. Nevertheless, metal-air batteries based on alkaline earth anodes have received limited attention and generally exhibit modest performance. In addition, many fundamental aspects of this system remain poorly understood, such as the reaction mechanisms associated with discharge and charging. The present study aims to close this knowledge gap and thereby accelerate the development of Mg/O_2 batteries by employing first-principles calculations to characterize electrochemical processes on the surfaces of likely discharge products, MgO and MgO_2. Thermodynamic limiting potentials for charge and discharge are calculated for several scenarios, including variations in surface stoichiometry and the presence/absence of intermediate species in the reaction pathway. The calculations indicate that pathways involving oxygen intermediates are preferred, as they generally result in higher discharge and lower charging voltages. In agreement with recent experiments, cells that discharge to MgO exhibit low round-trip efficiencies, which are rationalized by the presence of large thermodynamic overvoltages. In contrast, MgO_2-based cells are predicted to be much more efficient: superoxide-terminated facets on MgO_2 crystallites enable low overvoltages and round-trip efficiencies approaching 90%. These data suggest that the performance of Mg/O_2 batteries can be dramatically improved by biasing discharge toward the formation of MgO_2 rather than MgO.

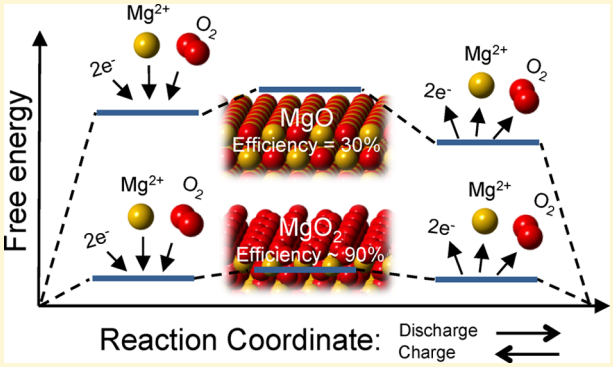

I. INTRODUCTION

The search for batteries with high energy densities suitable for electric vehicle applications has sparked interest in metal−oxygen electrochemistry.[1−4] One emerging metal−oxygen (or "metal-air") system is the magnesium−oxygen (Mg/O_2) battery. Such a battery is similar in concept to that of the well-studied lithium−oxygen (Li/O_2) system.[3,5−13] However, magnesium based systems potentially exhibit important advantages compared to Li analogues, such as an anode with higher volumetric capacity (3832 mAh cm^{-3} Mg vs 2062 mAh cm^{-3} Li) and suppressed dendrite formation, as well as lower cost.[14] Additionally, the theoretical energy density of the Mg/O_2 couple, 3.9 kWh/kg for a cell that discharges to magnesium oxide (MgO), lies above that of state-of-the-art Li-ion[15] and other metal−oxygen chemistries based on alkali metals, Figure 1.

Despite its promise, a Mg/O_2 cell that discharges to MgO is expected to be a difficult system to cycle, as MgO is chemically inert[16] and does not typically decompose under moderate conditions.[17] Shiga et al.[18,19] demonstrated a Mg/O_2 battery with a nonaqueous electrolyte. The discharge plateau of ∼1.1−1.2 V was attributed to the formation of MgO and is well below the theoretical voltage of 2.95 V. Decomposition of the

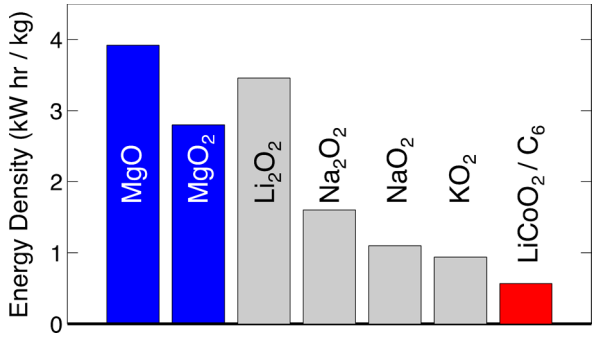

Figure 1. Theoretical specific energies (per mass of discharge product) of selected metal−oxygen chemistries (blue and gray bars) compared to Li-ion (red bar).[15]

Received: November 18, 2015
Revised: January 15, 2016
Published: February 11, 2016

DOI: 10.1021/acs.chemmater.5b04501
Chem. Mater. 2016, 28, 1390−1401

discharge product was not observed for charging potentials up to 3.2 V and at an elevated temperature of 60 °C, unless a redox mediator was employed. Additionally, Abraham[20] has described a Mg/O_2 battery with a discharge voltage between 0.7 and 1.1 V at room temperature.

Given the low discharge voltages and apparent irreversibility of MgO, a potentially more desirable discharge product is magnesium peroxide, MgO_2. The analogous Li/O_2 system provides support for this strategy, as it is now well established that cells that discharge to Li_2O_2 can be reversed with the application of moderate potentials, while those that form Li_2O cannot.[13,21−23] MgO_2 is metastable (with respect to MgO and O_2 gas) at ambient temperature and pressure. It is observed to decompose at 345 °C[24], and it is only marginally less favored thermodynamically than MgO: $\Delta G_f^0(MgO) = -568.9$ kJ/mol vs $\Delta G_f^0(MgO_2) = -567.8$ kJ/mol.[25,26] Our thermodynamic calculations suggest that MgO_2 becomes stable for temperatures below approximately −13 °C. Importantly, recent experiments involving Na/O_2 cells have shown that kinetic factors can play a role in determining the composition of the discharge phase. For example, Hartmann et al.[27] have observed that Na/O_2 cells discharge to sodium superoxide (NaO_2) despite the higher stability of the peroxide phase, Na_2O_2. Taken together, these data suggest that an Mg/O_2 battery that discharges to MgO_2 − rather than to MgO − could be possible, and may be desirable from the standpoint of reversibility.

The operation of an Mg/O_2 cell is expected to be governed by the following half-reactions at the anode and cathode:

Anode:

$$Mg \rightleftharpoons Mg^{2+} + 2e^- \quad (1)$$

Cathode:

$$Mg^{2+} + 2e^- + \frac{1}{2}O_2 \rightleftharpoons MgO, \quad U_0 = 2.95\ V \quad (2)$$

$$Mg^{2+} + 2e^- + O_2 \rightleftharpoons MgO_2, \quad U_0 = 2.94\ V \quad (3)$$

Here U_0 represents the theoretical cell voltage. MgO adopts the rock salt crystal structure with a lattice constant of 4.21 Å, whereas MgO_2 adopts the pyrite crystal structure with a lattice constant of 4.84 Å. Vannerberg has prepared the peroxide compound by treating MgO with hydrogen peroxide between 0 and 20 °C.[28] Vol'nov also prepared MgO_2 at room temperature using an aqueous solution of magnesium hydroxide and hydrogen peroxide, followed by drying with phosphorus pentoxide.[24] Magnesium superoxide, $Mg(O_2)_2$, has also been reported and was prepared using an ozone-saturated solution of Freon with MgO_2 suspended in the same media. The presence of the superoxide radical, O_2^-, was conformed by EPR spectra. X-ray diffraction on the yellowish $Mg(O_2)_2$ crystals indicated a rhombohedral crystal structure with lattice constants $a = 7.93$ Å and $\alpha = 93°$. Because $Mg(O_2)_2$ decomposes[29] at temperatures above −30 °C it is unlikely to be a viable candidate discharge product in an Mg/O_2 battery.

The present study aims to clarify the reaction mechanisms and energetics associated with charge and discharge of an Mg/O_2 cell. Density functional theory calculations, in combination with the method of Norskov et al.,[30−32] are used to predict the theoretical limiting potentials for several plausible reaction pathways. This method has previously been used to describe trends in electrochemical reactions in aqueous environments[33,34] and in metal/O_2 batteries based on Li,[35−37] Na,[38] Zn,[39] and Al.[40] Application to the Mg/O_2 system can facilitate an understanding of the origin of the low discharge voltage and irreversibility observed in prior experiments.[18,19] Such an analysis could also reveal strategies for improving performance.

Toward these goals, here we computationally examine discharge/charge reactions as a function of discharge product (MgO vs MgO_2), surface stoichiometry (stoichiometric vs oxygen-rich), and for pathways with and without intermediate phases. The calculations suggest that thermodynamic limitations are a major contributor to the low voltages observed in cells that discharge to MgO. In addition, they reveal that it is energetically favorable to reduce (i.e., during discharge) and evolve (i.e., during charging) oxygen via multistep pathways that involve intermediate, less-reduced species. In contrast to the poor performance predicted for MgO-based cells, discharging to an MgO_2 product along a pathway that involves electrochemistry on oxygen-rich (superoxide-terminated) surfaces yields the best combination of high discharge voltage and low charging voltage. In the absence of other transport or kinetic limitations, these data suggest that battery performance can be maximized via cathode designs or operating scenarios that favor the formation of an MgO_2 discharge product.

II. COMPUTATIONAL DETAILS

First-principles calculations were performed using the Vienna *ab initio* simulation package (VASP code).[41−44] The generalized gradient approximation (GGA) expressed with the formulation of Perdew−Burke−Ernzerhof (PBE) was used for the exchange-correlation energy.[45] Blochl's projector augmented wave method[46] was used to treat the core−valence electron interaction, with valence states of *2s* for Mg and *2s2p* for O. For calculations involving the conventional unit cell for bulk phases, the Brillouin zone was sampled with a Gamma-centered k-point mesh of 8 × 8 × 8 for oxides/peroxides and 16 × 16 × 16 for metals. The plane-wave cutoff energy was set to 520 eV, and a force tolerance of 0.01 eV/Å was used for all geometry optimizations. For bulk phases the cell shape, volume, and atom positions were relaxed; surface calculations employed in-plane lattice dimensions based on relaxation of the respective unit cell. To accommodate the large simulation cells necessary for calculations of reaction energies, a reduced plane-wave cutoff energy of 400 eV and force tolerance (0.04 eV/Å) were used in these cases. All calculations were spin polarized.

III. RESULTS AND DISCUSSION

A. Bulk Phases. The conventional cell of face centered cubic (FCC) MgO (space group: *Fm3m*) and pyrite MgO_2 (space group: *Pa3*) from Vannenburg[28] are illustrated in Figure 2. The calculated lattice constants for HCP Mg ($a = 3.19$ Å, $c = 5.18$ Å), MgO ($a = 4.24$ Å), and MgO_2 ($a = 4.88$ Å) are all in

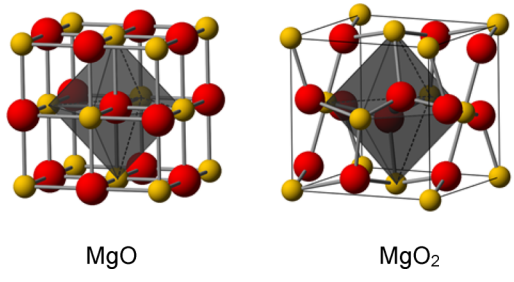

Figure 2. (Left) The rock salt crystal structure of MgO; oxygen is octahedrally coordinated by Mg. (Right) The pyrite crystal structure of MgO_2; the covalently bonded oxygen dimer (O_2) is octahedrally coordinated by Mg. Red spheres represent oxygen atoms; yellow spheres represent magnesium.

DOI: 10.1021/acs.chemmater.5b04501
Chem. Mater. 2016, 28, 1390−1401

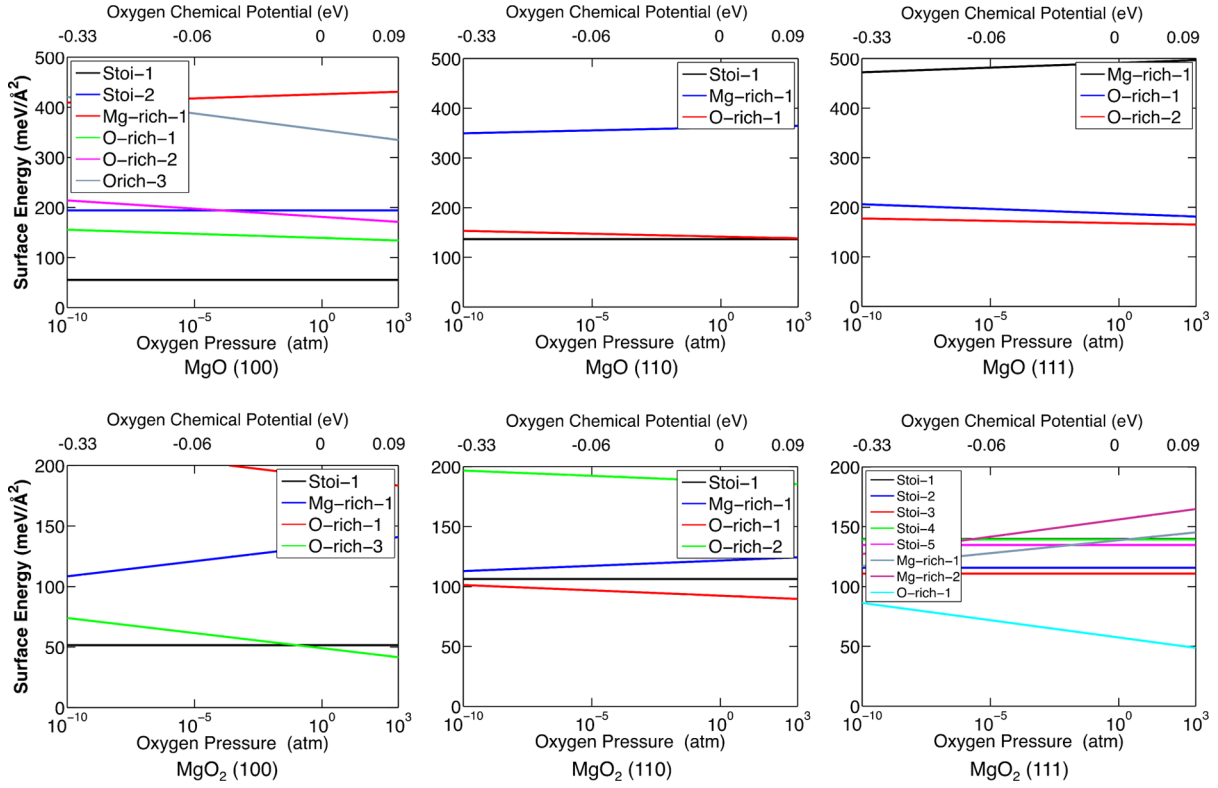

Figure 3. Surface free energies of MgO (top row) and MgO_2 (bottom row) as a function of oxygen chemical potential (top axis) and oxygen pressure (bottom axis) at 300 K. The notation "O-rich" and "Mg-rich" refer to the stoichiometry of the slabs. The chemical potential scale is defined to be zero at STP.

good agreement with experimental values: Mg (a = 3.21 Å, c = 5.20 Å),[47] MgO (a = 4.21 Å),[48] and MgO_2 (a = 4.84).[28] In MgO_2 the peroxide bond length was calculated to be 1.51 Å, which compares favorably with the value measured by X-ray diffraction, 1.50 Å.[28] An additional phase of interest is oxygen gas (O_2), for which we calculate a bond length of 1.23 Å, compared to the experimental value of 1.21 Å.[49]

B. Surface Stability. As described in more detail below, discharge and charge reactions are assumed to occur on the surfaces of MgO or MgO_2 discharge products. Modeling these reactions therefore requires knowledge of the low-energy facets of these compounds. Surface energies were evaluated for 31 distinct surface terminations of MgO and MgO_2 by cleaving along three low index directions: (100), (110), and (111). A vacuum region of 10 Å separated each of the two surfaces spanning a given slab, and both surfaces were identical, thereby avoiding spurious dipole interactions along the nonperiodic direction of the computational cell.

Surface energies were calculated using the methodology described by Reuter and Scheffler.[50] The most stable surface composition for a given cleavage direction will minimize the surface free energy

$$\gamma = \frac{1}{2A}(G^{\text{slab}} - \sum_i n_i\mu_i) \tag{4}$$

Here G^{slab} represents the energy of the surface slab, while n and μ are, respectively, the number and chemical potential of species i in the slab. A is the area of the surface, and the factor of 2 accounts for the double-sided slab model. The chemical potential of Mg (μ_{Mg}) and O_2 (μ_{O_2}) are linked by the expression

$$g_{\text{MgOx}} = \mu_{\text{Mg}} + (x/2)\mu_{O_2} \tag{5}$$

where g_{MgOx} refers to the energy per formula unit of MgO_x (x = 1, 2). The Gibbs free energy per oxygen atom, expressed as the chemical potential of an ideal gas at a temperature T and pressure p can be written as:

$$\mu_O(T, p) = \mu_O(T, p^0) + 1/2k_BT \ln(p/p^0) \tag{6}$$

Using eqs 4, 5, and 6, the surface energy at a fixed temperature can therefore be written as a function of oxygen chemical potential or O_2 pressure alone:

$$\gamma_{\text{MgOx}}(T, p, n_{\text{Mg}}, n_O) = \frac{1}{2A}\Big(G^{\text{slab}}(T, p, n_{\text{Mg}}, n_O) + (xn_{\text{Mg}} - n_O)\mu_O(T, p) - n_{\text{Mg}}g_{\text{MgO}_x}\Big) \tag{7}$$

We assume that oxygen in the gas phase is in equilibrium with oxygen dissolved in the battery's electrolyte.

To examine the relative stability of each MgO_x surface, the surface energy is plotted as a function of O_2 pressure and oxygen chemical potential. The chemical potential of oxygen gas at standard conditions (p^0 = 0.10 MPa, T^0 = 298.15 K) is defined as

$$\mu_{O_2} = \mu_{O_2}^{\text{DFT}} - \text{TS}_{\text{exp}} + (\Delta E^{\text{DFT}} - \Delta H_f^0) \tag{8}$$

where empirically determined entropy contributions (TS = 0.63 eV)[25] are included. Here the last term represents an empirical correction (applied on a per O_2 basis) evaluated as the difference between the calculated formation energy, ΔE^{DFT}, and the experimental enthalpy of formation, ΔH_f^0, for the compound in question (i.e., either MgO or MgO_2). These

DOI: 10.1021/acs.chemmater.5b04501
Chem. Mater. 2016, 28, 1390−1401

corrections − 1.46 eV/O_2 for MgO and 1.26 eV/O_2 for MgO_2 − are similar in spirit to those proposed elsewhere[36,51−53] and account for the well-known overbinding of O_2 gas, as well as for oxygen oxidation state errors. Contributions from pressure, vibrational energy, and entropy are neglected for solid phases.

The surface energies for all surfaces considered are summarized in Figure 3; ball-and-stick models of low energy structures appear in Figure 4. We first turn our attention to the

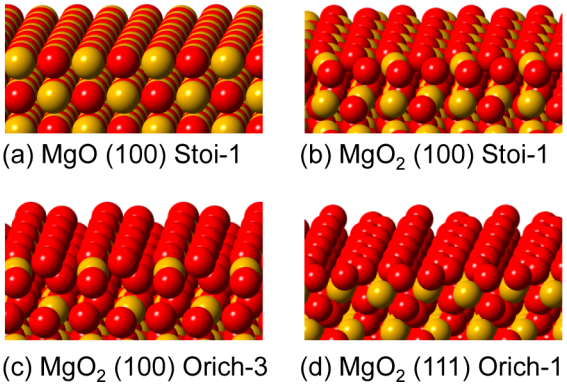

Figure 4. Most stable surface terminations for MgO and MgO_2. Red indicates oxygen atoms, and yellow indicates magnesium atoms.

surfaces of MgO (top row of Figure 3). In general, the most stable termination of rock salt-based compounds is the nonpolar (100) surface.[54] Consistent with this expectation, Figure 3 shows that the MgO (100) stoichiometric surface is the lowest in energy overall, with a calculated surface energy of 55 meV/Å^2. (The second most-stable MgO surface is the (110) stoichiometric surface, which has a much higher surface energy of 137 meV/Å^2.) Each oxygen atom in the stoichiometric (100) surface is coordinated by five Mg ions, and the in-plane Mg−O distance is the same as in the bulk, 2.12 Å.

The calculated and experimental surface energies for MgO (100) are summarized in Table 1. The experimentally

Table 1. Surface Energies for the Most Stable Surfaces of MgO and MgO_2 at Standard Conditions

surface	surface energy (meV/Å^2)
MgO (100)-Stoi-1 (this work)	55
MgO (100)-Stoi-1 (expt)[55]	72
MgO (100)-Stoi-1 (expt)[56]	83
MgO (100)-Stoi-1 (calc)[57]	56
MgO_2 (100)-Stoi-1	52
MgO_2 (100)-Orich-3	49
MgO_2 (111)-Orich-1	57

determined surface energy is expected to be slightly higher than the calculated value of a pristine surface due to the presence of different crystallographic planes and surface atom vacancies typical of real surfaces.[55−57]

Three nearly degenerate terminations comprise the stable surfaces of MgO_2, Figure 3 bottom panel. Two of these occur on the (111)-oriented facet and one on the (100) facet. The surface energies across all three fall within a narrow range from 49 to 57 meV/Å^2 and include the following (in order of increasing surface energy): oxygen-rich (100) 'Orich-3', stoichiometric (100) 'Stoi-1', and oxygen-rich (111) "Orich-1" (See Table 1). The stoichiometric surfaces have a 2:1 ratio of O to Mg atoms; for the Orich surfaces this ratio is greater than 2. More specifically, the surface layers of the Orich-1 and Orich-3 slabs have a stoichiometry with an O:Mg ratio of 4:1. In these cases the surface oxygen dimers have a bond length of 1.35 Å, a Bader charge of approximately −1, and a nonzero magnetic moment. These features are consistent with the presence of a superoxide-like surface layer.[29] Below this surface layer the electronic structure quickly reverts to peroxide-like behavior, with O_2 bond lengths of 1.51 Å, Bader charges consistent with the presence of O_2^{2-}, and the absence of a magnetic moment.

The calculated surface energies were used to predict the equilibrium crystallite shapes for MgO and MgO_2 via the Wulff construction,[58] shown in Figure 5. For MgO, the stoichiometric

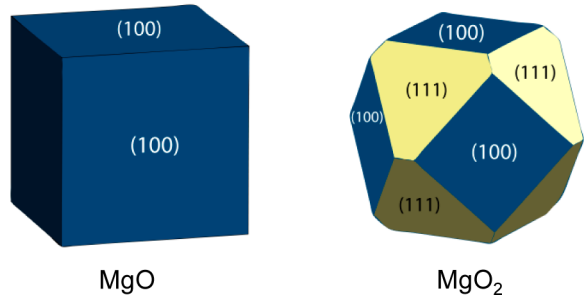

Figure 5. Equilibrium crystallite shapes predicted from the Wulff construction.

(100) surface comprises the entire surface area of the crystallite. In contrast, two facets, (100) and (111), comprise the surface area of the MgO_2 crystallite, which is a 14-sided tetradecagon. The yellow (111) facet comprises 54% of the surface area, and the blue (100) facet covers the remaining 46%. Given the slightly lower energies associated with the Orich-1 and Orich-3 terminations (Table 1), we expect that the surfaces of MgO_2 crystallites will be predominantly oxygen-rich, with a superoxide-like surface layer.

Having established the stable surfaces of MgO and MgO_2, the electrochemistry associated with discharge and charge reactions occurring on these surfaces was subsequently examined.

C. Reaction Energies. *Review of the Theoretical Limiting Potential Method and Its Application to the MgO (100) Surface.* Limiting potentials were evaluated for two reaction pathways (described below) involving discharge/charge reactions on MgO (100), following the approach of Norskov et al.[30,32,35,36,59−62] This treatment models the discharge process as a series of adsorption events onto the surface of an existing particle of the discharge product.

For illustrative purposes, Figure 6 presents a generic discharge process. In the present case the surface is assumed to be the stable Stoi-1 (100) surface of MgO. The surface is modeled using a 2 × 2 expansion of the primitive surface cell. In this geometry each surface layer contains 8 formula units of MgO. We define a "complete" discharge reaction pathway as consisting of the consecutive adsorption or deposition of 8 additional MgO formula units. At the completion of this process the thickness of the surface slab will have increased by two single formula-unit layers; atoms are added to each face of the slab so as to maintain identical surfaces. In a similar fashion, recharge can be modeled by the sequential removal of individual molecules or atoms from the surfaces.

DOI: 10.1021/acs.chemmater.5b04501
Chem. Mater. 2016, 28, 1390−1401

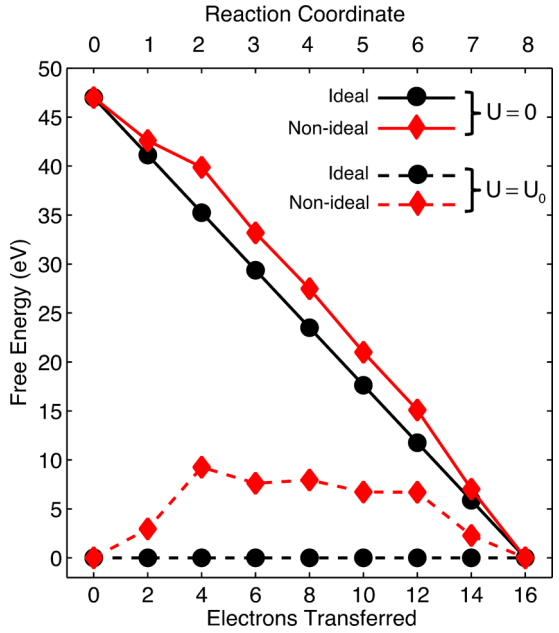

Figure 6. Prototypical discharge reactions. Black curves represent an ideal reaction pathway depicted at zero applied voltage, $U = 0$ (solid line), and at an applied voltage $U = U_0$ equal to the cell's theoretical voltage (dashed line). The reaction is considered ideal because the voltage associated with each elementary step is equal to the theoretical voltage associated with the formation energy of the discharge product. For comparison, the red curves depict a nonideal reaction plotted at $U = 0$ (solid) and $U = U_0$ (dashed).

Each step in the discharge or charging sequence is referred to as an "elementary electrochemical step." During a discharge step, two electrons are transferred from the Mg anode to the cathode, where they reduce oxygen; reduced oxygen can then also combine with an Mg^{2+} cation. (Similarly, during charging two electrons are removed.) The energy change associated with each elementary step i is given by the free energy of reaction $\Delta G_{rxn,i} = G_{products} - G_{reactants}$. During discharge, $G_{products}$ refers to the energy of the (neutral) species adsorbed on MgO (100); for example, these may be Mg^0, MgO, MgO_2, *etc.* The energy of the reactants, $\Delta G_{reactants}$, is given by a combination of the MgO slab (including any species adsorbed in previous steps) and magnesium and oxygen atoms in an appropriate reference state. The chemical potential of magnesium is taken to be that of HCP magnesium metal (i.e., equal to the chemical potential of the Mg anode), and the chemical potential of oxygen is that of oxygen gas at STP. As previously mentioned, this reference state assumes that oxygen dissolved in the electrolyte is in equilibrium with gas-phase oxygen. With this definition, the energy change associated with an elementary electrochemical (discharge) step, $\Delta G_{rxn,i}$, corresponds to the adsorption energy for an adatom of $Mg^0 = Mg^{2+} + 2e^-$, or of a molecule of MgO_x.

We note that the sum of all elementary reaction energies must equal the free energy associated with the growth of (two) formula-unit layers on the slab's surfaces:

$$\Delta G^{layer} = -\sum \Delta G^{elementary}_{rxn,i} \tag{9}$$

The energy of the initial configuration (i.e., before discharge) corresponds to reaction coordinate 0 of Figure 6 (red or black solid lines) and is equal to the sum of the energies of the bare surface layer and the energy of all magnesium and oxygen atoms in the reservoir. During discharge, each subsequent reaction at the surface reduces the free energy of the system until all reactants have been adsorbed, corresponding to a free energy which is equal to zero by definition (see reaction coordinate 8 in Figure 6). Each change in free energy associated with an elementary discharge step is evaluated as

$$\Delta G^{elem}_{rxn,i} = G^{step}(n^*_{Mg}, m^*_O) - \{G^{step}_{previous} + n_{Mg}\mu_{Mg} + m_O\mu_O\} \tag{10}$$

where $G^{step}(n^*, m^*)$ refers to the energy of the slab supercell after n_{Mg} and m_O, ions (respectively) have adsorbed on the surface. Likewise, $G^{step}{}_{previous}$ is the total energy of the computational cell from the previous step. The last two terms in equation 10 refer to the energies of magnesium and oxygen atoms that remain in the reservoir.

In principle, many different reaction pathways may be followed during discharge or charge. Here, two plausible pathways are examined. (For simplicity, the examples below are described assuming a discharge pathway.) The pathways include the following: (*i.*) A "single step" pathway where oxygen is reduced to a 2^- oxidation state through a one-step reaction

$$(Mg^{2+} + 2e^-) + \frac{1}{2}O_2 + * \rightleftharpoons MgO^* \tag{11}$$

and (*ii.*) a multistep pathway wherein oxygen is reduced incrementally to a 2^- oxidation state via two consecutive reduction reactions. The initial deposition results in the formation of an adsorbed peroxide intermediate molecule (MgO_2); a subsequent deposition of Mg^{2+} combined with transfer of 2 additional electrons forms 2 formula units of adsorbed MgO:

$$(Mg^{2+} + 2e^-) + O_2 + * \rightleftharpoons MgO_2^* \tag{12a}$$

$$MgO_2^* + (Mg^{2+} + 2e^-) \rightleftharpoons 2MgO^* \tag{12b}$$

Here a lone asterisk denotes a surface site, while a superscript asterisk denotes a surface-adsorbed species.

The forward direction in the preceding reactions involve oxygen reduction (ORR) and the precipitation of a solid MgO_x discharge product, while the reverse corresponds to the oxygen evolution reaction (OER) and the dissolution of that product during charging. In both pathways the elementary reactions (eq 11 or 12a + 12b) are repeated until a full surface layer has been added (discharge) or removed (charge). The disassociation of O_2 at the surface is not taken into account as this is a kinetic process, and the present formalism is concerned only with thermodynamics.

The multistep reaction mechanism 12a + 12b is motivated by the thermodynamic theory of electron transfer.[63] In this pathway charge is temporarily "stored" in an intermediate, peroxide adsorbed species (MgO_2^*) on the way to achieving a final oxidation state of 2^- in MgO*. The peroxide intermediate has a higher oxidation state (i.e., it is less reduced compared to the oxide) wherein each oxygen atom has an effective charge of 1^-. The present computational approach has previously been used to elucidate the important role played by intermediate species in other electrochemical processes, such as hydrogen evolution and oxidation,[63] oxygen evolution and reduction,[59,64] and carbon dioxide reduction.[65]

We emphasize that all steps in reactions 11 and 12a + 12b are electrochemical steps that involve electron transfer. Although some studies have included nonelectrochemical (i.e., chemical)

DOI: 10.1021/acs.chemmater.5b04501
Chem. Mater. 2016, 28, 1390−1401

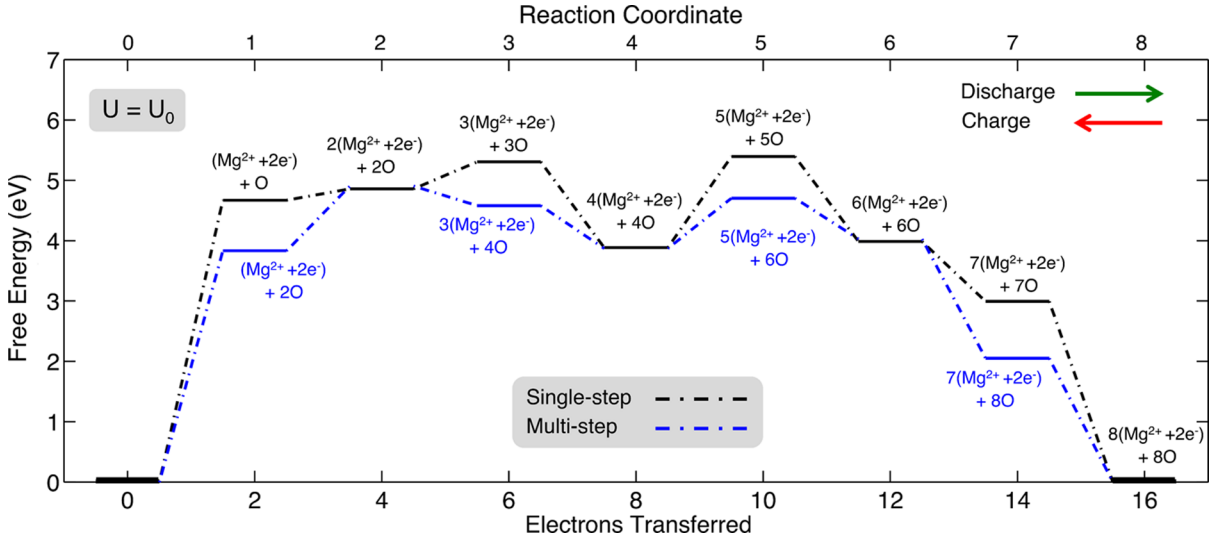

Figure 7. Calculated free energy diagram for discharge (read left-to-right) and charging (read right-to-left) of an Mg/O_2 cell, assuming that all reactions occur on the MgO (100) surface. The black line refers to the single step pathway of eq 11; the blue line refers to the multistep pathway, eqs 12a and 12b. All energies are plotted assuming the application of a potential, U, equal to the theoretical cell voltage, $U = U_0$. The identity of the species that are adsorbed on the surface during each elementary discharge reaction is indicated with text; these same species are desorbed during charging. A total of 8 Mg^{2+} ions, 8 oxygen atoms, and 16 electrons are added to the surface to replicate its initial structure.

steps in their analyses,[38,66] chemical steps are potential-independent and therefore do not contribute to the useful electrical work supplied by the cell during discharge. For this reason we focus only on electrochemical steps.

MgO (100) Single-Step Reaction. The black line in Figure 7 depicts the free energy profile for the single step reaction pathway of reaction 11. Reaction coordinate zero corresponds to the state before both charge transfer and deposition onto the MgO (100) surface (i.e., this is the "clean" surface). Similarly, reaction coordinate 8 corresponds to the final surface; this surface is equivalent to the initial surface except that the slab has grown thicker via the deposition of two formula-unit layers. As each layer corresponds to the addition of 8 Mg and 8 O ions, a total of 16 electrons are transferred per layer.

For each elementary step in the discharge sequence a search over possible deposition locations on the surface is carried out. Once identified, the lowest energy adsorption site is occupied, and its energy is recorded; the next deposition event then takes place in the presence of the adsorbate deposited in the previous step. At each step all atoms on the surface are relaxed to their minimum-force positions.

For discharge to be spontaneous each elementary electrochemical step i must be "downhill", i.e., $\Delta G_{rxn,i} < 0$. For an idealized discharge mechanism, $\Delta G_{rxn,i}$ for each step will be equal to the formation energy, $\Delta G_f(MgO)$ of bulk MgO. When the energy of each elementary step is plotted vs the number of electrons transferred, this idealized scenario yields a straight line comprised of 8 identical line segments, as shown using the solid black line in Figure 6. Each segment corresponds to an elementary deposition step during the growth of a single formula-unit layer on the MgO (100) surface.

The slope of each segment, which is equal to that of the full line, is the theoretical cell voltage associated with the formation energy of bulk MgO through the Nernst equation

$$U_0 = -\frac{\Delta G_f^{bulk}}{e\nu_{e^-}} \tag{13}$$

where e is the charge of an electron, and ν_e is the stoichiometric coefficient (2) associated with the number of electrons in the reaction. Such an idealized discharge mechanism would exhibit zero thermodynamic overvoltage.

Of course in a real system the energy change associated with an elementary discharge step need not be equal to the bulk formation energy: surface heterogeneity and deposition events that do not deposit a stoichiometric formula unit can result in energy changes $\Delta G_{rxn,i}$ which are greater or less than that for the formation energy of bulk MgO. During discharge, reactions steps whose energy change is less exergonic than $\Delta G_f(MgO)$ contribute to the discharge overvoltage. According to Norskov's definition, the least exergonic of these steps along a given reaction pathway is defined as the potential determining step. This step defines the limiting potential for discharge, $U^{discharge}$:

$$U^{discharge} = \min\left|\frac{\Delta G_{rxn,i}(U=0)}{e\nu_{e^-}}\right| \tag{14}$$

Here, the "min" function selects the elementary reaction that is the least exergonic.

During charging all elementary reaction steps should be endergonic. Steps having a free energy change which are more endergonic than the decomposition free energy of bulk MgO contribute to the charging overvoltage. Following Norskov's definition, the most "uphill" of these steps is defined as the potential determining step, with a limiting potential of

$$U^{charge} = \max\left|\frac{\Delta G_{rxn,i}(U=0)}{e\nu_{e^-}}\right| \tag{15}$$

A key goal in generating a free energy diagram such as Figure 7 is to identify the potential determining steps for charge and discharge. These predictions provide information regarding the expected efficiency of an Mg/O_2 cell. Moreover, by comparing the reaction energies associated with different reaction pathways it may be possible to identify thermodynamically favorable mechanisms. To assist in identifying the limiting potentials, it is helpful to plot the free energy diagram at an

DOI: 10.1021/acs.chemmater.5b04501
Chem. Mater. 2016, 28, 1390−1401

Table 2. Calculated Limiting Potentials, Thermodynamic Overvoltages, and Efficiencies Associated with Various Discharge and Charging Reactions in an Mg/O_2 Cell[a]

	limiting potential (V)		overvoltage (V)		
discharge product, surface, and reaction mechanism	discharge	charge	discharge	charge	voltaic efficiency (%)
MgO (100) Stoi [single-step]	0.70	4.45	2.25	1.50	16
MgO (100) Stoi [multistep]	1.15	3.98	1.80	1.03	29
MgO_2 (100) Stoi [single-step]	0.92	4.69	2.02	1.75	20
MgO_2 (100) Stoi [multistep]	1.31	4.04	1.63	1.10	33
MgO_2 (111) Orich-1 [single-step]	2.76 (2.61)	3.01 (3.25)	0.18 (0.33)	0.07 (0.31)	92 (80)
MgO_2 (100) Orich-3 [single-step]	2.83 (2.63)	3.27 (3.29)	0.11 (0.31)	0.33 (0.35)	87 (80)
Li_2O_2 (ref 37)			0.35, 0.68	0.20, 0.40	

[a]Values in regular text refer to terrace-site reactions; values in parentheses refer to nonterrace reactions, which are limiting only for the superoxide-terminated surfaces, Orich-1 and Orich-3.

applied potential equal to the theoretical voltage of the cell, i.e., $U = U_0$. For an Mg/O_2 cell that discharges to MgO this would correspond to a voltage of 2.95 V (eq 2). This applied voltage shifts the energy of electrons present in the discharge pathway by eU_0 and thereby also shifts the electrochemical potential of magnesium such that it is the same in the anode and cathode. (In other words, the applied voltage exactly counteracts the thermodynamic driving force for discharge.) In this case the idealized pathway described previously (Figure 6) would appear as a horizontal line at zero on the free energy diagram, i.e., $\Delta G_{rxn,i}(U = U_0) = 0$, for all steps since the change in free energy associated with every elementary reaction is opposed by the bias potential. The black dashed line in Figure 6 illustrates this scenario.

For an actual (i.e., nonideal) discharge pathway plotted at $U = U_0$, free energy changes associated with elementary reaction steps will appear as a sequence of uphill and downhill steps; this is illustrated by the red dashed line in Figure 6. As previously mentioned, the nonideal nature of a pathway arises from differences in the composition of the species adsorbed in successive steps and from heterogeneity in the surface adsorption sites.

Following this convention, potential determining steps can be straightforwardly identified as uphill steps in the reaction pathway when plotting with an applied bias of $U = U_0$. Thus, for charge or discharge, an elementary reaction with a positive reaction energy, $\Delta G_{rxn,i}(U_0) > 0$, can be associated with a limiting potential. The magnitude of the uphill step is proportional to the amount of "lost" or "unharvested" energy during discharge or the amount of additional energy input required for charge. The largest of these steps over the entire pathway is defined as the potential determining step

$$\max[\Delta G_{rxn,i}(U = U_0)] = \eta e \nu_{e^-} \quad (16)$$

This step determines the "thermodynamic overvoltage," η, which is defined as the difference in the theoretical cell voltage and the limiting potential:

$$\eta^{discharge} = U_0 - U^{discharge}, \quad \eta^{charge} = U^{charge} - U_0 \quad (17)$$

Note that the limiting potential is always an uphill step when plotting at $U = U_0$. For discharge, it is the largest uphill step when reading the reaction energy profile from left-to-right; for recharge it is the largest step reading right-to-left.

Referring now to the single-step pathway (eq 11), during discharge single Mg and O atoms are deposited on the (100) surface at each step. Energy levels for each step are shown in Figure 7. As each reaction coordinate represents the minimum energy configuration of reactants and products, the diagram is equally valid for charging (right-to-left). The potential determining step for discharge is the initial deposition event, corresponding to the transfer of the first 2 electrons of a formula unit of MgO* onto an empty (100) terrace. The voltage U^{dis} associated with the step (eq 14) is very low, only 0.70 V. Subsequently, steps 2−7 represent reactions at low-coordinated sites such as islands, steps, kinks, *etc.* These steps all exhibit larger voltages (i.e., liberate more energy during discharge) than the initial reaction. That the initial deposition of MgO is the potential determining step can be understood based on simple bond counting: deposition onto a flat terrace presents the geometry with the fewest available neighbors for bonding.

For recharge, the potential determining step is the initial dissolution of a single formula unit of MgO* from the (100) terrace, corresponding to reaction coordinate 8 to 7 in Figure 7. This reaction results in the formation of a vacancy or pit on an otherwise pristine terrace. The formation of this feature is energetically costly because dissolution from a filled terrace layer requires the most bonds to be broken. This step has a large limiting potential of U^{chg} = 4.45 V (eq 15). Subsequent reaction steps − coordinates 7 through 2 − correspond to the dissolution of MgO* at low-coordinated sites. These steps occur at much lower applied voltages.

Combining the calculated limiting potentials with the theoretical cell voltage, eq 17, yields large overvoltages for both discharge and charge: $\eta^{discharge}$ = 2.25 V and η^{charge} = 1.50 V. Consequently, the voltaic efficiency for this pathway, defined as U^{dis}/U^{chg}, is very low, only 16%. A summary of the calculated limiting potentials, overvoltages, and efficiencies for the MgO (100) single-step pathway is given in Table 2.

MgO (100) Multistep Reaction. The blue line in Figure 7 depicts the free energy profile for the multistep reaction pathway given by eq 12a and 12b. In this pathway two reaction steps are required to reduce oxygen to a nominal charge state of 2^-. The first step corresponds to the deposition of MgO_2*. This is followed by the deposition of $(Mg^{2+} + 2e^-)$*, which further reduces the two oxygen atoms to the oxidation state of bulk MgO. This sequence is then repeated 3 more times, until a full monolayer is deposited.

The multistep pathway is slightly more efficient than the single-step pathway: It increases the limiting discharge potential from 0.70 V to U^{dis} = 1.15 V and reduces the limiting charge potential from 4.45 V to U^{chg} = 3.98 V. The increase (decrease) in discharge (charging) potential indicates that it is thermodynamically more favorable for oxygen to be reduced (oxidized) via a pathway that involves the multistep reduction

DOI: 10.1021/acs.chemmater.5b04501
Chem. Mater. 2016, 28, 1390−1401

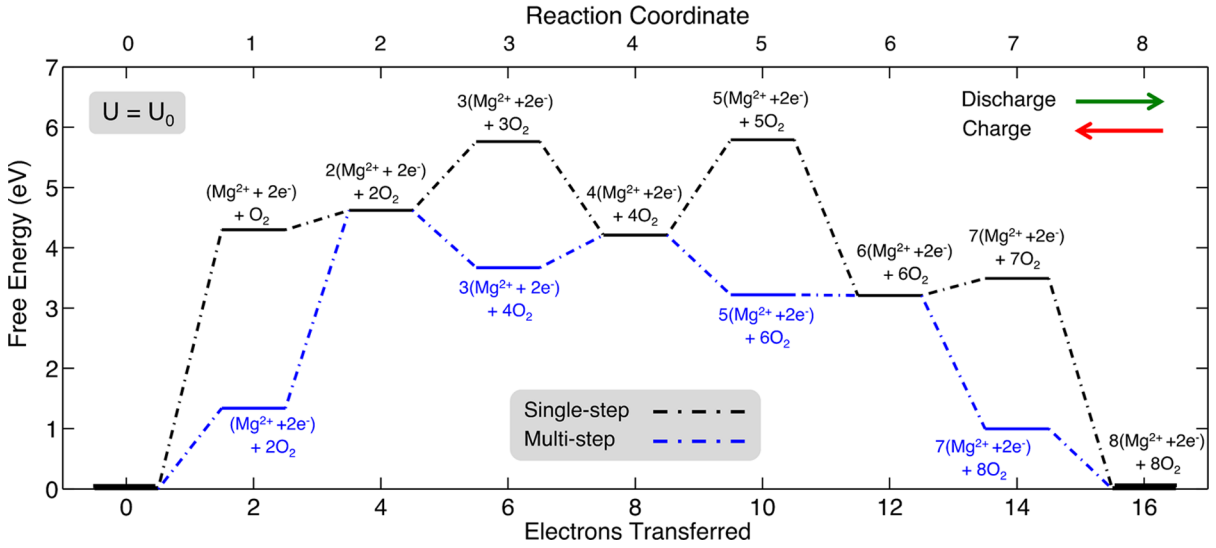

Figure 8. Calculated free energy diagram for discharge and charging of an Mg/O_2 cell, assuming that all reactions occur on the stoichiometric MgO_2 (100) surface. Black lines refer to the single step pathway, eq 18; blue lines refer to the multistep pathway, eqs 19a and 19b. Energies are plotted assuming the application of a potential, U, equal to the theoretical cell potential, $U = U_0$.

(oxidation) of oxygen, with MgO_2* as an intermediate. Consequently, the multistep mechanism increases the voltaic efficiency to 29%. Similarly, the thermodynamic overvoltages for discharge and charge are nearly 0.5 V smaller than for the single-step mechanism: $\eta^{discharge}$ = 1.80 V and η^{charge} = 1.03 V.

Shiga et al.[18,19] reported a Mg/O_2 battery with a discharge voltage of approximately 1.1−1.2 V. Assuming an MgO discharge product, this voltage is in good agreement with the limiting potential calculated for the multistep pathway, U^{dis} = 1.15 V. Similarly, their attempts to recharge the cell[18,19] revealed that the discharge product did not decompose at potentials as large as the oxidative stability limit of the electrolyte (~3.2 V). This is also consistent with the limiting potential calculated for the multistep pathway, which suggests that a minimum voltage of ~4 V is needed to initiate the oxygen evolution reaction.

MgO_2 (100) Stoichiometric Surface. Given that the formation energies of MgO and MgO_2 are very similar, it is conceivable that an Mg/O_2 cell could discharge to MgO_2 rather than to MgO. Discharge mechanisms that form MgO_2 may also exhibit faster kinetics than those leading to MgO, as the former does not require the disassociation of O_2. To examine whether such a pathway would be beneficial from the standpoint of thermodynamics, the limiting potentials on the stoichiometric MgO_2 (100) surface were evaluated. As done for the MgO calculations described above, a 2 × 2 expansion of the primitive surface cell was adopted. In this geometry each surface layer contains 8 formula units of MgO_2; a "complete" discharge reaction therefore consists of the consecutive adsorption of 8 additional formula units.

Two reaction pathways were considered; these include: (*i.*) a "single step" pathway wherein a full MgO_2 formula unit is created at each elementary step

$$(Mg^{2+} + 2e^-) + O_2 + * \rightleftharpoons MgO_2* \quad (18)$$

and (*ii.*) a multistep pathway where the initial deposition of an intermediate magnesium superoxide $Mg(O_2)_2$* unit is followed by the deposition of $(Mg^{2+} + 2e^-)$*. This pathway generates two formula units of MgO_2* for every pair of 2 e^- transfers:

$$(Mg^{2+} + 2e^-) + 2O_2 + * \rightleftharpoons Mg(O_2)_2* \quad (19a)$$

$$Mg(O_2)_2* + (Mg^{2+} + 2e^-) \rightleftharpoons 2MgO_2* \quad (19b)$$

Reactions 19a and 19b are repeated until the surface has grown by one formula-unit layer.

The black line in Figure 8 depicts the free energy profile for the single-step reaction pathway, eq 18. The same methodology and bias potential (i.e., $U = U_0$, where U_0 reflects the theoretical voltage associated with formation of bulk MgO_2) described previously was used. As seen for the MgO pathways, the potential determining step for discharge (charge) corresponds to the deposition (dissolution) of a formula unit on (from) a flat terrace. The calculated discharge voltage is low, U^{dis} = 0.92 V. Similarly, the voltage needed for charging is high, U^{chg} = 4.69 V. The large difference in discharge/charge voltages results in a poor voltaic efficiency of 20% (Table 2).

The blue line in Figure 8 depicts the free energy profile for the multistep reaction pathway, eqs 19a and 19b. Similar to the pathways discussed previously, the potential determining step for discharge occurs early in the reaction sequence, from step 1 to 2, corresponding to the deposition of $(Mg^{2+}+2e^-)$* near the previously deposited $Mg(O_2)_2$* species on an otherwise empty terrace. For charge, the potential is determined by the dissolution of $Mg(O_2)_2$* corresponding to step 7 to 6. The multistep reaction increases the discharge voltage to U^{dis} = 1.31 V and reduces the charging voltage to U^{chg} = 4.04 V. These voltages correspond to an approximately 0.4−0.6 V improvement over the single-step pathway and are reflected in an increase in the efficiency from 20% to 33%, Table 2. The trend of higher efficiency for the multistep pathway on the MgO_2 (100) surface mimics what was observed previously on MgO (100). The similarity of these results suggest that reaction pathways involving intermediate charge states may in general be more efficient for ORR and OER in metal/oxygen batteries.[38,51,52,67]

MgO_2 Superoxide-Terminated Surface. Our discussion has thus far focused on reactions occurring on stoichiometric surfaces. We now shift attention to pathways on the oxygen-rich (111) "Orich-1" and (100) 'Orich-3' surfaces, which are

DOI: 10.1021/acs.chemmater.5b04501
Chem. Mater. 2016, 28, 1390−1401

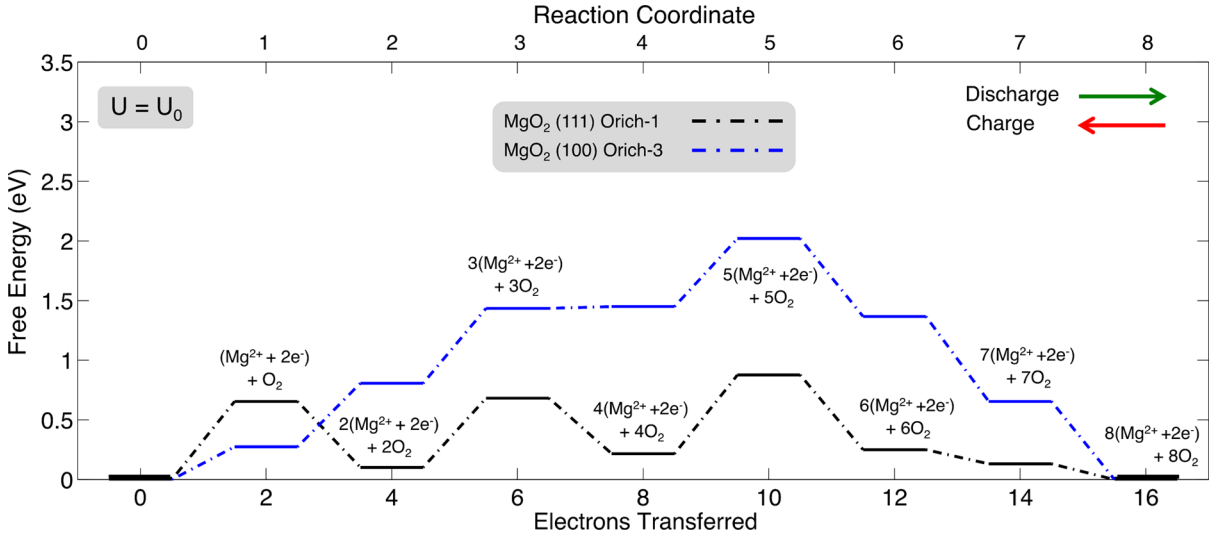

Figure 9. Calculated free energy diagram for discharge and charging of an Mg/O_2 cell, for single-step reactions (eq 18) occurring on the oxygen rich MgO_2 (111) "Orich-1" (black curve) and MgO_2 (100) 'Orich-3' (blue curve) surfaces. Energies are plotted assuming the application of a potential, U, equal to the theoretical cell potential, $U = U_0$. (Note that the maximum value for the ordinate (3.5 eV) used in this plot is half the value used in Figures 7 and 8.)

expected to appear on the surfaces of MgO_2 crystallites (Table 1, Figure 5), as they are the most stable terminations overall. As previously described, these surfaces contain superoxide moieties on the surface layer. Reaction energies for the Orich-1 surface were evaluated using a 2 × 1 expansion of the primitive surface cell. In this geometry each surface layer contains 8 formula units of MgO_2.

The reaction pathway for discharge/charge on the Orich-1 surface is shown in Figure 9 for the single-step mechanism of eq 18. The calculated limiting potentials on this surface are significantly closer to the theoretical cell voltage than for any of the foregoing systems: U^{dis} = 2.61 V and U^{chg} = 3.25 V, Table 2. These potentials occur at reaction step 4→5 for discharge and at step 6→5 for charging. Indeed, this reaction pathway is nearly ideal, as suggested by its approximately flat profile in Figure 9 (cf. black dashed line in Figure 6). These potentials yield a round-trip efficiency of 80%.

The limiting potentials for pathways on the stoichiometric MgO and MgO_2 surfaces discussed earlier largely arise from terrace-based reactions. Due to their high concentration it has been suggested that, terrace sites likely comprise the majority of sites accessed at the high current densities required for automotive applications.[37,40] Restricting our analysis of the Orich-1 surface only to terrace-site reactions results in a further reduction in overvoltages [0.18 (0.07) V for discharge (charge), Table 2] and a correspondingly higher efficiency of 92%.

Reaction energies on the (100) Orich-3 superoxide surface were also evaluated using the single-step mechanism of eq 18 and are shown in Figure 9. Similar to the Orich-1 surface, the calculated limiting potentials are close to the theoretical cell voltage: U^{dis} = 2.63 V and U^{chg} = 3.29 V, resulting in a high round-trip efficiency of 80%. The limiting potential for discharge occurs from step 2→3, while the limiting potential for charge occurs from step 7→6. Restricting the analysis to terrace sites, we find that discharge is expected at a slightly higher potential, U^{dis} = 2.83 V, while the charging potential is mostly unchanged, U^{chg} = 3.27 V. These potentials yield a slightly higher round-trip efficiency of 87%, with low overvoltages of 0.11 V and 0.33 V, Table 2.

Discussion. We note that the favorable electrochemistry on both of the superoxide-terminated surfaces occurs for a single-step reaction mechanism, eq 18. This may seem counterintuitive given that our earlier calculations on the stoichiometric surfaces of MgO and MgO_2 suggested that intermediate-containing pathways (eq 12 and eq 19, respectively) exhibit more favorable thermodynamics than single-step pathways. In fact, the superoxide surfaces appear to be a special case of this rule, which emerges from the distinct nature of their surface charge state relative to the bulk. In support of this hypothesis we recall that oxygen dimers in the bulk regions of these slabs exhibit a peroxide-like charge state, as determined by a Bader charge and bond-length analysis; on the other hand, the surface dimers exist in a superoxide-like state. Analysis of changes to the charge state of the slab before and after an elementary discharge step reveal that the $2e^-$ transferred according to eq 18 are split between an existing surface O_2, reducing it into a peroxide, and the newly adsorbed O_2, which is a superoxide. Thus, the net amount of bulk peroxide increases, while maintaining the superoxide surface layer. In contrast to the multistep reactions (eq 12 and eq 19), where a separate step is devoted to the formation of a (less-reduced) intermediate species, here the less-reduced superoxide surface moieties can be considered as a permanently present intermediate species. In other words, the slab's superoxide surface layer serves as a "built-in" intermediate.

Our calculations suggest that discharge/charge reactions are much more efficient when they occur on the superoxide-terminated, oxygen-rich surfaces of MgO_2 than when they occur on stoichiometric surfaces, regardless of whether the latter belong to an oxide (MgO) or peroxide (MgO_2) discharge product. Recent experiments on Mg/O_2 batteries support this assertion: high overpotentials were observed in MgO-based cells,[18,19] whereas lower overpotentials and higher rechargeability were reported for a cell having a mixed MgO/MgO_2 discharge product.[68]

For the superoxide-terminated surfaces overvoltages are approximately 0.3 V or smaller, while for stoichiometric surfaces values in excess of 1 V are typical. This trend is

DOI: 10.1021/acs.chemmater.5b04501
Chem. Mater. 2016, 28, 1390−1401

consistent with the behavior of metal oxygen batteries that discharge to superoxides, such as those based on potassium[69] and sodium anodes.[27,70] These superoxide-based cells exhibit much lower overvoltages than those that discharge to a peroxide.[70,71] It has been suggested[27,69] that the greater reversibility of the superoxide systems can be traced to more efficient reduction and oxidation of oxygen. In superoxide-based cells these processes occur via a single electron transfer ($O_2 + Na^+ + 1e^- \leftrightarrow NaO_2$), whereas two electrons must be exchanged for a peroxide product ($O_2 + 2Na^+ + 2e^- \leftrightarrow Na_2O_2$). These experimental observations, in combination with the present calculations, suggest that the precipitation/dissolution of superoxide-based discharge products − be they stoichiometric superoxides or superoxide-terminated peroxides − should be intrinsically more efficient than the cycling of stoichiometric peroxide- or oxide-based discharge products.

As previously mentioned, our calculations find that intermediate-containing reaction pathways are favored as they generally maximize discharge voltages and lower charging voltages. This observation is consistent with the thermodynamic theory of multielectron transfer reactions. As described by Koper,[63] and based on Marcus theory, the simultaneous transfer of two electrons − which could in principle occur during the reduction of oxygen upon formation of an MgO discharge product − requires an activation energy which is four times larger than that needed for a single electron transfer. Consequently, a series of sequential, single electron transfers is expected to present a more energetically favorable pathway for such a reaction. The latter mechanism can be realized by temporarily "storing" charge from the first single electron transfer in an intermediate species, such as MgO_2, wherein oxygen is less reduced than in the final MgO product. A second single electron transfer subsequently converts MgO_2 to MgO. A similar pathway is proposed for cells that discharge to MgO_2, except that magnesium superoxide, $Mg(O_2)_2$, now serves as the intermediate.

It should be noted that the preceding description is based on kinetics, while the present study is based solely on a thermodynamic analysis of reaction energies. A link between thermodynamics and kinetics is provided by the Brønsted−Evans−Polanyi relationship,[72] which correlates the *energy of* reaction with the *activation energy* for that reaction. Hence, our (thermodynamic) observation that reaction pathways containing less-reduced intermediate species are favored is consistent with the system avoiding pathways that exhibit high activation energies that can arise from unfavorable simultaneous multielectron transfers. Several studies have noted the presence or importance of intermediate species in reactions occurring in metal−oxygen batteries[51,67] or in other contexts.[59,62,64,65]

Finally, it is instructive to compare the present results for an Mg/O_2 cell to studies on the Li/O_2 system.[35−37,66,73] A recent report by Viswanathan et al.[37] calculated overvoltages for terrace site reactions on the Li_2O_2 discharge product of 0.35 and 0.68 V for discharge and 0.2 and 0.4 V for charging, Table 2. These values are slightly larger than the overvoltages calculated here for the oxygen-rich surfaces of MgO_2, which range from 0.11 to 0.18 V for discharge and 0.07 to 0.33 V for charging. Based on thermodynamics alone, this implies that an Mg/O_2 cell that discharges to MgO_2 could be more efficient than a Li/O_2 cell.

IV. CONCLUSIONS

A rechargeable battery based on an Mg/O_2 couple presents an attractive chemistry due to its high theoretical energy density and potential for low cost. Nevertheless, few experimental studies of this system exist, and in all cases these studies report performance that is far from the ideal: high overpotentials and limited cycleability are commonly observed. In addition, many fundamental aspects of this system remain poorly understood, such as the reaction mechanisms associated with discharge and charge. Lacking this understanding, improvements to Mg/O_2 batteries will be limited to approaches based on trial-and-error.

To accelerate the development of Mg/O_2 batteries, the present study employs Density Functional Theory calculations to characterize discharge/charge mechanisms on the surfaces of plausible discharge products, MgO and MgO_2. These compounds have similar formation energies, and recent experiments have shown that both can be present following discharge of an Mg/O_2 cell.[68] Thermodynamic limiting potentials for charge and discharge were calculated for several scenarios, including variations in surface stoichiometry and the presence/absence of intermediate species in the reaction pathway.

Based on these calculations we conclude the following: (*i.*) Reaction pathways that include (less-reduced) oxygen intermediates are more efficient than those that do not. These intermediate-containing pathways generally maximize discharge voltages and lower charging voltages. This conclusion is consistent with the thermodynamic theory of multielectron transfer reactions.[63] (*ii.*) Due to the presence of large thermodynamic overvoltages, cells that discharge to MgO are expected to exhibit intrinsically poor performance. The calculated discharge/charge voltages of 1.15/∼4.0 V are consistent with recent experiments,[18,19] which show that MgO-based cells exhibit low round-trip efficiencies. (*iii.*) In contrast, MgO_2-based cells are predicted to be much more efficient: the superoxide-terminated facets of MgO_2 crystallites allow for high discharge/low charging voltages, resulting in round-trip efficiencies approaching 90%. The possibility for improved performance in MgO_2-based cells is supported by a recent experiment which observed higher discharge voltages in a cell having a mixed MgO/MgO_2 discharge product.[68]

In turn, these observations suggest the following design directions for Mg/O_2 batteries: (*i.*) Maximum energy density can theoretically be achieved with a cell that reversibly cycles MgO (Figure 1). However, surface-mediated reactions on MgO are shown by the present calculations to be highly inefficient and should be avoided. Consequently, for an MgO-based cell to be viable a liquid-phase reaction pathway, likely in combination with a redox mediator, is preferred. Whether this pathway can be realized at high current densities − where many metal/O_2 systems transition to a surface-mediated mechanism/film-like morphology − remains an open question. (*ii.*) An alternative strategy is to bias the discharge so as to produce MgO_2 rather than MgO. As described above, surface-mediated reactions on the former compound are suggested by our calculations to be much more efficient than those on the latter. Increasing the oxygen pressure and/or reducing the temperature of the cell during operation could achieve such an outcome. The relative stability of MgO_2 vs MgO could also be tuned by varying the composition of the electrolyte or the cathode support. Additional study is needed to examine the effectiveness of these strategies.

DOI: 10.1021/acs.chemmater.5b04501
Chem. Mater. 2016, 28, 1390−1401

AUTHOR INFORMATION

Corresponding Author

*Phone: 734-764-4808. E-mail: djsiege@umich.edu.

Notes

The authors declare no competing financial interest.

ACKNOWLEDGMENTS

J.G.S. and D.J.S. gratefully acknowledge financial support from DENSO Corporation. D.J.S. acknowledges DTU Energy, the Villum Foundation's Visiting Professor Program, and the Nordea Foundation's Residence Program for support during his stay at DTU.

REFERENCES

(1) Imanishi, N.; Luntz, A.; Bruce, P. *The Lithium Air Battery: Fundamentals*; Springer: New York, 2014.

(2) Radin, M. D.; Siegel, D. J. Non-Aqueous Metal-Air Batteries: Past, Present, and Future. Chapter 18. In *Rechargeable Batteries: Materials, Technologies and New Trends*; Zhang, Z., Zhang, S. S., Eds.; Springer: Switzerland, 2015; pp 511−539.

(3) Bruce, P. G.; Freunberger, S. A.; Hardwick, L. J.; Tarascon, J.-M. Li-O_2 and Li-S Batteries with High Energy Storage. *Nat. Mater.* **2012**, *11*, 19−29.

(4) Christensen, J.; Albertus, P.; Sanchez-Carrera, R. S.; Lohmann, T.; Kozinsky, B.; Liedtke, R.; Ahmed, J.; Kojic, A. A Critical Review of Li/Air Batteries. *J. Electrochem. Soc.* **2012**, *159*, R1−R30.

(5) Girishkumar, G.; McCloskey, B.; Luntz, A. C.; Swanson, S.; Wilcke, W. Lithium−Air Battery: Promise and Challenges. *J. Phys. Chem. Lett.* **2010**, *1*, 2193−2203.

(6) Radin, M. D.; Monroe, C. W.; Siegel, D. J. Impact of Space-Charge Layers on Sudden Death in Li/O_2 Batteries. *J. Phys. Chem. Lett.* **2015**, *6*, 3017−3022.

(7) Kumar, N.; Radin, M. D.; Wood, B. C.; Ogitsu, T.; Siegel, D. J. Surface-Mediated Solvent Decomposition in Li-Air Batteries: Impact of Peroxide and Superoxide Surface Terminations. *J. Phys. Chem. C* **2015**, *119*, 9050−9060.

(8) Griffith, L. D.; Sleightholme, A. E. S.; Mansfield, J. F.; Siegel, D. J.; Monroe, C. W. Correlating Li/O_2 Cell Capacity and Product Morphology with Discharge Current. *ACS Appl. Mater. Interfaces* **2015**, *7*, 7670−7678.

(9) Radin, M. D.; Monroe, C. W.; Siegel, D. J. How Dopants Can Enhance Charge Transport in Li_2O_2. *Chem. Mater.* **2015**, *27*, 839−847.

(10) Tian, F.; Radin, M. D.; Siegel, D. J. Enhanced Charge Transport in Amorphous Li_2O_2. *Chem. Mater.* **2014**, *26*, 2952−2959.

(11) Radin, M. D.; Siegel, D. J. Charge Transport in Lithium Peroxide: Relevance for Rechargeable Metal−air Batteries. *Energy Environ. Sci.* **2013**, *6*, 2370−2379.

(12) Radin, M. D.; Tian, F.; Siegel, D. J. Electronic Structure of Li_2O_2 {0001} Surfaces. *J. Mater. Sci.* **2012**, *47*, 7564−7570.

(13) Radin, M. D.; Rodriguez, J. F.; Tian, F.; Siegel, D. J. Lithium Peroxide Surfaces Are Metallic, While Lithium Oxide Surfaces Are Not. *J. Am. Chem. Soc.* **2012**, *134*, 1093−1103.

(14) Muldoon, J.; Bucur, C. B.; Oliver, A. G.; Sugimoto, T.; Matsui, M.; Kim, H. S.; Allred, G. D.; Zajicek, J.; Kotani, Y. Electrolyte Roadblocks to a Magnesium Rechargeable Battery. *Energy Environ. Sci.* **2012**, *5*, 5941−5950.

(15) Zu, C.-X.; Li, H. Thermodynamic Analysis on Energy Densities of Batteries. *Energy Environ. Sci.* **2011**, *4*, 2614−2624.

(16) Wichtendahl, R.; Ha, U.; Kuhlenbeck, H.; Freund, H. TDS Study of the Bonding of CO and NO to Vacuum-Cleaved NiO (100). *Surf. Sci.* **1999**, *423*, 90−98.

(17) Muldoon, J.; Bucur, C. B.; Gregory, T. Quest for Nonaqueous Multivalent Secondary Batteries: Magnesium and Beyond. *Chem. Rev.* **2014**, *114*, 11683−11720.

(18) Shiga, T.; Hase, Y.; Kato, Y.; Inoue, M.; Takechi, K. A Rechargeable Non-Aqueous Mg-O2 Battery. *Chem. Commun.* **2013**, *49*, 9152−9154.

(19) Shiga, T.; Hase, Y.; Yagi, Y.; Takahashi, N.; Takechi, K. Catalytic Cycle Employing a TEMPO − Anion Complex to Obtain a Secondary Mg − O_2 Battery. *J. Phys. Chem. Lett.* **2014**, *5*, 1648−1652.

(20) Abraham, K. M. A Brief History of Non-Aqueous Metal-Air Batteries. *ECS Trans.* **2006**, *3*, 67−71.

(21) Xu, W.; Xu, K.; Viswanathan, V. V.; Towne, S. A.; Hardy, J. S.; Xiao, J.; Nie, Z.; Hu, D.; Wang, D.; Zhang, J. G. Reaction Mechanisms for the Limited Reversibility of Li-O_2 Chemistry in Organic Carbonate Electrolytes. *J. Power Sources* **2011**, *196*, 9631−9639.

(22) Obrovac, M. N.; Dunlap, R. A.; Sanderson, R. J.; Dahn, J. R. The Electrochemical Displacement Reaction of Lithium with Metal Oxides. *J. Electrochem. Soc.* **2001**, *148*, A576−A588.

(23) Poizot, P.; Laruelle, S.; Grugeon, S.; Dupont, L.; Tarascon, J.-M. Nano-Sized Transition-Metal Oxides as Negative-Electrode Materials for Lithium-Ion Batteries. *Nature* **2000**, *407*, 496.

(24) Volnov, I.; Latysheva, E. Thermal Stability of Magnesium Peroxide. *Izv. Akad. Nauk SSSR* **1970**, *1*, 13−18.

(25) Chase, M. W. *NIST-JANAF Thermochemical Tables*, 4th ed.; Am. Institute Phys.: 1998.

(26) Coughlin, J. Contributions to the Data of Theoretical Metallurgy. *Bur. Mines* **1953**, *X11*.

(27) Hartmann, P.; Bender, C. L.; Vračar, M.; Dürr, A. K.; Garsuch, A.; Janek, J.; Adelhelm, P. A Rechargeable Room-Temperature Sodium Superoxide (NaO_2) Battery. *Nat. Mater.* **2013**, *12*, 228−232.

(28) Vannerberg, N. The Formation and Structure of Magnesium Peroxide. *Ark. Kemi* **1959**, *14*, 99−105.

(29) Vol'nov, I. I.; Tokareva, S. A.; Belevskii, V. N.; Latysheva, E. I. The Formation of Magnesium Perperoxide in the Reaction of Magnesium Peroxide with Ozone. *Bull. Acad. Sci. USSR, Div. Chem. Sci.* **1970**, *19*, 468−471.

(30) Nørskov, J. K.; Rossmeisl, J.; Logadottir, A.; Lindqvist, L.; Kitchin, J. R.; Bligaard, T.; Jonsson, H. Origin of the Overpotential for Oxygen Reduction at a Fuel-Cell Cathode. *J. Phys. Chem. B* **2004**, *108*, 17886−17892.

(31) Greeley, J.; Stephens, I. E. L.; Bondarenko, A. S.; Johansson, T. P.; Hansen, H. A.; Jaramillo, T. F.; Rossmeisl, J.; Chorkendorff, I.; Nørskov, J. K. Alloys of Platinum and Early Transition Metals as Oxygen Reduction Electrocatalysts. *Nat. Chem.* **2009**, *1*, 552−556.

(32) Man, I. C.; Su, H.-Y.; Calle-Vallejo, F.; Hansen, H. A.; Martínez, J. I.; Inoglu, N. G.; Kitchin, J.; Jaramillo, T. F.; Nørskov, J. K.; Rossmeisl, J. Universality in Oxygen Evolution Electrocatalysis on Oxide Surfaces. *ChemCatChem* **2011**, *3*, 1159−1165.

(33) Greeley, J.; Jaramillo, T. F.; Bonde, J.; Chorkendorff, I. B.; Nørskov, J. K. Computational High-Throughput Screening of Electrocatalytic Materials for Hydrogen Evolution. *Nat. Mater.* **2006**, *5*, 909−913.

(34) Nørskov, J. K.; Bligaard, T.; Rossmeisl, J.; Christensen, C. H. Towards the Computational Design of Solid Catalysts. *Nat. Chem.* **2009**, *1*, 37−46.

(35) Hummelshøj, J. S.; Blomqvist, J.; Datta, S.; Vegge, T.; Rossmeisl, J.; Thygesen, K. S.; Luntz, A. C.; Jacobsen, K. W.; Nørskov, J. K. Communications: Elementary Oxygen Electrode Reactions in the Aprotic Li-Air Battery. *J. Chem. Phys.* **2010**, *132*, 071101−071104.

(36) Hummelshøj, J. S.; Luntz, A. C.; Nørskov, J. K. Theoretical Evidence for Low Kinetic Overpotentials in Li-O_2 Electrochemistry. *J. Chem. Phys.* **2013**, *138*, 034703−034712.

(37) Viswanathan, V.; Norskov, J. K.; Speidel, A.; Scheffler, R.; Gowda, S.; Luntz, A. C. Li−O_2 Kinetic Overpotentials: Tafel Plots from Experiment and First-Principles Theory. *J. Phys. Chem. Lett.* **2013**, *4*, 556−560.

(38) Lee, B.; Seo, D.-H.; Lim, H.-D.; Park, I.; Park, K.-Y.; Kim, J.; Kang, K. First-Principles Study of the Reaction Mechanism in Sodium−Oxygen Batteries. *Chem. Mater.* **2014**, *26*, 1048−1055.

(39) Siahrostami, S.; Tripković, V.; Lundgaard, K. T.; Jensen, K. E.; Hansen, H. a; Hummelshøj, J. S.; Mýrdal, J. S. G.; Vegge, T.; Nørskov, J. K.; Rossmeisl, J. First Principles Investigation of Zinc-Anode Dissolution in Zinc-Air Batteries. *Phys. Chem. Chem. Phys.* **2013**, *15*, 6416−6421.

DOI: 10.1021/acs.chemmater.5b04501
Chem. Mater. 2016, 28, 1390−1401

(40) Chen, L. D.; Norskov, J. K.; Luntz, A. C. Al − Air Batteries: Fundamental Thermodynamic Limitations from First-Principles Theory. *J. Phys. Chem. Lett.* **2015**, *6*, 175−179.
(41) Kresse, G.; Furthmuller, J. Efficiency of Ab-Initio Total Energy Calculations for Metals and Semiconductors Using a Plane-Wave Basis Set. *Comput. Mater. Sci.* **1996**, *6*, 15−50.
(42) Kresse, G.; Hafner, J. Ab Initio Molecular Dynamics for Liquid Metals. *Phys. Rev. B: Condens. Matter Mater. Phys.* **1993**, *47*, 558−561.
(43) Kresse, G.; Hafner, J. Ab Initio Molecular-Dynamics Simulation of the Liquid-Metal-Amorphous-Semiconductor Transition in Germanium. *Phys. Rev. B: Condens. Matter Mater. Phys.* **1994**, *49*, 14251−14269.
(44) Kresse, G.; Furthmüller, J. Efficient Iterative Schemes for Ab Initio Total-Energy Calculations Using a Plane-Wave Basis Set. *Phys. Rev. B: Condens. Matter Mater. Phys.* **1996**, *54*, 11169−11186.
(45) Perdew, J.; Burke, K.; Ernzerhof, M. Generalized Gradient Approximation Made Simple. *Phys. Rev. Lett.* **1996**, *77*, 3865−3868.
(46) Blochl, P. E. Projector Augmented-Wave Method. *Phys. Rev. B: Condens. Matter Mater. Phys.* **1994**, *50*, 17953−17979.
(47) Straumanis, M. E. The Precision Determination of Lattice Constants by the Powder and Rotating Crystal Methods and Applications. *J. Appl. Phys.* **1949**, *20*, 726.
(48) Smith, D. K.; Leider, H. R. Low-Temperature Thermal Expansion of LiH, MgO and CaO. *J. Appl. Crystallogr.* **1968**, *1*, 246−249.
(49) Lide, D. R. *CRC Handbook of Chemistry and Physics*, 87th ed.; 1992.
(50) Reuter, K.; Scheffler, M. Composition, Structure, and Stability of RuO_2(110) as a Function of Oxygen Pressure. *Phys. Rev. B: Condens. Matter Mater. Phys.* **2001**, *65*, 035406.
(51) Kang, S.; Mo, Y.; Ong, S. P.; Ceder, G. A Facile Mechanism for Recharging Li_2O_2 in Li − O_2 Batteries. *Chem. Mater.* **2013**, *25*, 3328−3336.
(52) Kang, S.; Mo, Y.; Ong, S. P.; Ceder, G. Nanoscale Stabilization of Sodium Oxides: Implications for Na-O2 Batteries. *Nano Lett.* **2014**, *14*, 1016−1020.
(53) Christensen, R.; Hummelshøj, J. S.; Hansen, H. A.; Vegge, T. Reducing Systematic Errors in Oxide Species with Density Functional Theory Calculations. *J. Phys. Chem. C* **2015**, *119*, 17596−17601.
(54) Tasker, P. W. The Stability of Ionic Crystal Surfaces. *J. Phys. C: Solid State Phys.* **1979**, *12*, 4977−4984.
(55) Westwood, A. R. C.; Goldheim, D. L. Cleavage Surface Energy of {100} Magnesium Oxide. *J. Appl. Phys.* **1963**, *34*, 3335.
(56) Hayun, S.; Tran, T.; Ushakov, S. V.; Thron, A. M.; van Benthem, K.; Navrotsky, A.; Castro, R. H. R. Experimental Methodologies for Assessing the Surface Energy of Highly Hygroscopic Materials: The Case of Nanocrystalline Magnesia. *J. Phys. Chem. C* **2011**, *115*, 23929−23935.
(57) Bajdich, M.; Nørskov, J. K.; Vojvodic, A. Surface Energetics of Alkaline-Earth Metal Oxides: Trends in Stability and Adsorption of Small Molecules. *Phys. Rev. B: Condens. Matter Mater. Phys.* **2015**, *91*, 155401−155410.
(58) Strickland-Constable, R. F. *Kinetics And Mechanisms of Crystallization*; Academic Press: London and New York, 1968.
(59) Rossmeisl, J.; Logadottir, a.; Nørskov, J. K. Electrolysis of Water on (oxidized) Metal Surfaces. *Chem. Phys.* **2005**, *319*, 178−184.
(60) Rossmeisl, J.; Qu, Z. W.; Zhu, H.; Kroes, G. J.; Nørskov, J. K. Electrolysis of Water on Oxide Surfaces. *J. Electroanal. Chem.* **2007**, *607*, 83−89.
(61) Valdés, Á.; Qu, Z. W.; Kroes, G. J.; Rossmeisl, J.; Nørskov, J. K. Oxidation and Photo-Oxidation of Water on TiO2 Surface. *J. Phys. Chem. C* **2008**, *112*, 9872−9879.
(62) Hansen, H. A.; Rossmeisl, J.; Nørskov, J. K. Surface Pourbaix Diagrams and Oxygen Reduction Activity of Pt, Ag and Ni(111) Surfaces Studied by DFT. *Phys. Chem. Chem. Phys.* **2008**, *10*, 3722−3730.
(63) Koper, M. T. M. Thermodynamic Theory of Multi-Electron Transfer Reactions: Implications for Electrocatalysis. *J. Electroanal. Chem.* **2011**, *660*, 254−260.
(64) Viswanathan, V.; Hansen, H. A.; Rossmeisl, J.; Nørskov, J. K. Universality in Oxygen Reduction Electrocatalysis on Metal Surfaces. *ACS Catal.* **2012**, *2*, 1654−1660.
(65) Angamuthu, R.; Byers, P.; Lutz, M.; Spek, A. L.; Bouwman, E. Electrocatalytic CO_2 Conversion to Oxalate by a Copper Complex. *Science* **2010**, *327*, 313−315.
(66) Mo, Y.; Ong, S. P.; Ceder, G. First-Principles Study of the Oxygen Evolution Reaction of Lithium Peroxide in the Lithium-Air Battery. *Phys. Rev. B: Condens. Matter Mater. Phys.* **2011**, *84*, 205446.
(67) Lu, Y.; Shao-horn, Y. Probing the Reaction Kinetics of the Charge Reactions of Nonaqueous Li-O_2 Batteries. *J. Phys. Chem. Lett.* **2013**, *4*, 93−99.
(68) Vardar, G.; Nelson, E. G.; Smith, J. G.; Naruse, J.; Hiramatsu, H.; Bartlett, B. M.; Sleightholme, A. E. S.; Siegel, D. J.; Monroe, C. W. Identifying the Discharge Product and Reaction Pathway for a Secondary Mg/O_2 Battery. *Chem. Mater.* **2015**, *27*, 7564−7568.
(69) Ren, X.; Wu, Y. A Low-Overpotential Potassium-Oxygen Battery Based on Potassium Superoxide. *J. Am. Chem. Soc.* **2013**, *135*, 2923−2926.
(70) Mccloskey, B. D.; Garcia, J. M.; Luntz, A. C. Chemical and Electrochemical Differences in Nonaqueous Li−O_2 and Na−O_2 Batteries. *J. Phys. Chem. Lett.* **2014**, *5*, 1230−1235.
(71) Sun, Q.; Yang, Y.; Fu, Z.-W. Electrochemical Properties of Room Temperature Sodium−air Batteries with Non-Aqueous Electrolyte. *Electrochem. Commun.* **2012**, *16*, 22−25.
(72) Nørskov, J. K.; Bligaard, T.; Hvolbæk, B.; Abild-Pedersen, F.; Chorkendorff, I.; Christensen, C. H. The Nature of the Active Site in Heterogeneous Metal Catalysis. *Chem. Soc. Rev.* **2008**, *37*, 2163−2171.
(73) Viswanathan, V.; Thygesen, K. S.; Hummelshøj, J. S.; Nørskov, J. K.; Girishkumar, G.; McCloskey, B. D.; Luntz, a C. Electrical Conductivity in Li_2O_2 and Its Role in Determining Capacity Limitations in Non-Aqueous Li-O_2 Batteries. *J. Chem. Phys.* **2011**, *135*, 214704.

DOI: 10.1021/acs.chemmater.5b04501
Chem. Mater. 2016, 28, 1390−1401